G. Le Besnerais, F. Champagnat, P. Cornic, A. Plyer, B. Leclaire, A. Cheminet, C. Illoul, G. Losfeld, Y. Le Sant, D. Donjat, F. Nicolas, F. Micheli
(ONERA)

E-mail: guy.le_besnerais@onera.fr

DOI: 10.12762/2016.AL12-09

Experimental Fluid Mechanics goes 3D: New Numerical Methods for Quantitative Instantaneous 3D Imagery of Fluids

We review recent developments made between three departments at ONERA (DTIM, DAFE, DMAE) with regard to 3D imagery used in fluid mechanics experiments. We first discuss 3D PIV (Particle Image Velocimetry) and present original contributions on the modeling of the imaging process, the reconstruction of the 3D volume of particles and the estimation of the 3D motion field between two time instants. These three contributions emphasize the pointwise character of particles in PIV, in contrast with classical Tomo-PIV approaches, and have been shown to outperform state-of-the-art methods, yielding more accurate 3D velocity estimations. Then, we consider 3DBOS (Background Oriented Schlieren), which is aimed at estimating the instantaneous 3D density field of a moving fluid. We have recently proposed an original one-step numerical approach for 3DBOS. This method has been successfully used in several experiments conducted in various ONERA facilities, in particular in the F2 and S1MA wind tunnels. Finally, we draw some important perspectives, especially for the study of compressible flows by combining both techniques.

Introduction

Over the last decade, new imaging set-ups and numerical methods aimed at 3D field measurement for fluid mechanics have been developed. In its most common form, tomographic PIV, introduced in [19], uses 4 cameras (or more) to reconstruct volumes of particles and derive the instantaneous 3D velocity field by 3D correlation. 3DBOS [1][32] is an extension of Background Oriented Schlieren, which allows the reconstruction of the instantaneous 3D density volume of flows, again by combining images recorded by several (usually more than ten) synchronized cameras.

Being instantaneous and volumetric, these 3D field measurement techniques yield unprecedented information on the flows under study. Indeed, before they were proposed, field characterization in fluid mechanics was only possible either in an instantaneous sense, but limited to 2D (for instance, in plane PIV, see our companion paper in this volume [27]), or could be obtained on 3D domains as well, but in a time-averaged sense (for instance, by scanning space with a pointwise sensor, e.g., by Hot-Wire Anemometry or Laser Doppler Velocimetry). Flows of industrial interest, in particular in the aerospace domain, are characterized by high Reynolds numbers and often also high Mach numbers. As such, they inherently exhibit a three-dimensional structure due to turbulence, not mentioning the increased complexity of the systems (three-dimensional model geometries, active flow control by mechanical or fluidic actuators, etc.). The characterization of complex unsteady three-dimensional flow structures thus appears to be essential to investigate problems of industrial relevance. Finally, from the theoretical point of view, 3D field measurement techniques offer the potential to take a major step towards the complete understanding of complex flows. As an example, they allow the measurement of the velocity gradient and, in particular, the vorticity, which provide information of major importance in wake vortex characterization and, more generally, regarding turbulence studies.

Nevertheless, 3D field measurement also brings several tedious issues from the experimental and numerical point of view. We focus here on the latter point and present original developments made between three departments at ONERA (DTIM, DAFE and DMAE) aimed at achieving more efficient and accurate data processing methods. In both the 3DPIV and 3DBOS contexts, our contributions build on a reformulation of the problem, a careful examination of its experimental conditions and limitations, and lead to new algorithm proposals.

The paper is organized as follows: we first consider 3DPIV and present several methodological contributions made since 2013. The second part of the paper describes the original 3DBOS reconstruction developed since 2012 and recently validated in several facilities at ONERA. Perspectives of these works and opportunities for joint studies between 3DPIV and 3DBOS are outlined in the last section.

3D PIV

Introduction

Recalling 2D PIV

PIV (Particle Image Velocimetry) is a measurement process where two images of a plane in a flow are recorded at two close time instants and correlated, in order to produce an estimated displacement field. This recording uses pulsed laser illumination and often high-speed cameras. The processing basically consists in seeking corresponding small regions (or interrogation windows, IW) in the two images, by optimizing some intensity-based criterion. Numerous algorithms have been proposed for this operation; see [38] for a review. In 2009, some of the authors of this paper proposed a fast parallel algorithm called FOLKI-SPIV [5], whose GPU implementation reached unprecedented performance: dense displacement fields on 4K images are computed in less than 0.2 s. FOLKI-SPIV runtime is faster than the time required for loading the images from the camera. Hence, when processing PIV image sequences, computation becomes actually transparent compared to storage.

Before turning to 3D PIV, some basic facts and constraints on 2D PIV should be briefly recalled. First, in most PIV settings related to aerodynamic studies, unless microscopic viewing conditions are used, the seeding particles appear as point sources for the cameras (in optics, they are said to be unresolved by the cameras). As a consequence, their actual shape in the image stems from the characteristics of the imaging process. This process is essentially controlled by the experimenter, through the tuning of the parameters of the illumination system and of the camera. Ideally, one aims at recording particles in the form of Gaussian-shaped images with diameters of 2-3 pixels, so as to minimize localization uncertainty and aliasing effects. In the end, the actual spatial resolution of PIV estimated displacement fields depends on two main parameters: the size of the IW and the density of particles. 10 particles per IW is recognized as a good rule-of-thumb to ensure the correct behavior of the correlation process, and, in this case, the spatial resolution is given by the size of the IW projected onto the illuminated plane [38].

Tomo-PIV

The main idea behind Tomo-PIV, which was first proposed in [19], is to extend the principle of PIV, *i.e.*, the cross-correlation of two 2D images of seeded flows, to 3D. Hence, one needs to acquire two "3D images" of the flow, in order to cross-correlate them to produce a 3D displacement field. In Tomo-PIV, each of these "3D images" is actually a volume representation obtained by tomographic reconstruction from several simultaneous 2D images of some illuminated 3D area of the flow. This operation is usually formulated as the iterative estimation of a volume, discretized over a large number of 3D grid cells (or voxels). It is important to recall that this tomographic process was originally designed to provide a representation of the actual volume of particles *suitable for correlation*. Hence, the same prescription as that concerning the 2D imaging process in PIV has been followed: the voxel size Δ is usually aligned with the pixel size ($v/p = 1$) and particles in the reconstructed volume appear ideally as 2-3 voxel-wide Gaussian-shaped blobs. This approach leads to the observation model outlined in the left part of Figure 1, where images result from the integration of a 3D intensity field along rays. The modeling of this integration process and the concatenation of the equations associated with all pixels of all cameras lead to a linear system, $I = WE$. In this equation, image intensities I_k on pixels k are related to volume intensities $E_n = E(n\Delta)$ through a weighting matrix W_{kn}, which is non-negative and sparse.

Given that most Tomo-PIV settings use 4 cameras (but systems with 6 or 8 cameras have also been described), the previous system is severely underdetermined – in a 4-cameras system there can be two orders of magnitude less of recorded data (I_k) than there are voxel values (E_n). Prior information on the reconstructed volume is essential here. All Tomo-PIV methods are based upon the hypothesis that the density of seeding particles is low, so that voxel intensities are most often zero and take on positive values only in the vicinity of the particles – and there are very few of these visible. In order to enforce these properties in the reconstructed volume, multiplicative algorithms, such as MART and SMART, originating from Computerized Tomography, are popular choices and their action is often restricted to "valid" voxels selected in an initial process such as MLOS [2].

The main and most studied factor affecting the performance of Tomo-PIV methods is the density of particles, which is usually evaluated in terms of a non-dimensional number, which is a projected representation of the seeding density: the average number of particles per pixel (ppp) recorded on the camera CCD sensor. The ppp is linked to the spatial resolution: the higher the ppp is, the better the resolution is. However, higher densities lead to a dramatic increase of "ghost particles", *i.e.*, false positives related to matching ambiguities of indiscernible particle images. A good trade-off between ghosts and spatial resolution is typically found at around 0.05 ppp [39].

However, we have demonstrated in simulation studies [7][8] that several other factors – often neglected in performance evaluation studies – affect the quality of the tomographic reconstruction. The "added background particles", *i.e.*, particles that are visible to the cameras but not accounted for in the reconstruction, have been identified as a source of ghost particles in [19]. The authors attribute these added particles to the Gaussian profile of the laser sheet or to uncontrolled light reflections, thus implying that a proper experiment could avoid them. However, we have demonstrated from simple geometrical considerations that added particles are unavoidable in Tomo-PIV. Indeed, while the reconstruction is done in the intersection volume of the camera field of view, all cameras also record particles lying in the union of the fields of view and not in the intersection. These added particles act as a strong source of noise in the reconstruction because multiplicative inversion algorithms such as MART or SMART strive to explain their images by ghost particles in the intersection volume.

Another important factor that has only recently been identified is the defocusing occurring when trying to image volumes with cameras having a limited depth of field [40]. By means of a thorough simulation study [8], we have shown that neglecting the defocus in the imaging model leads to a significant increase in the number of missed detections. It is a strong motivation for designing new reconstruction frameworks, where defocus effects could be modeled and accounted for more easily, such as the one presented in the next Section.

Particle Volume Reconstruction (PVR)

As already mentioned, the observation model behind usual Tomo-PIV methods does not correspond to a physical model of the actual imaging process. The latter is illustrated in the right part of Figure 1. A particle can be considered as a 3D point source located at some 3D position, whose image is a "point-spread function" (PSF) centered on a 2D point given by the geometrical model of the camera. Most often, PSF are modeled as truncated Gaussian functions, parameterized by their standard deviation σ_{psf}. As a result, the image appears as the sum of P PSF functions, as in Equation (1), where x denotes the 2D position in the image plane, X_p is the 3D position of the p-th particle, h is the PSF function (which, in the general case, depends on the 3D position of the particle because of defocus effects) and F is the projective transformation from the 3D world to a 2D image, identified by the calibration.

$$I(x) = \Sigma_{p=1}^{P} E_p h_{X_p}\left(x - F\left(X_p\right)\right) \qquad (1)$$

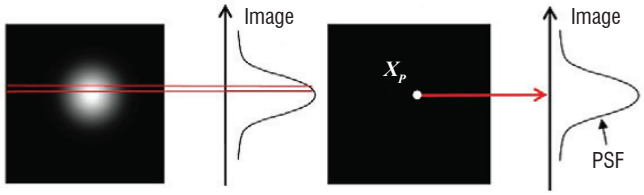

Figure 1 – Image formation models for 3DPIV. Traditional Tomo-PIV methods such as [19] are based on the "blob" model (left). In the proposed PVR model (right), particles are point sources for the camera, their image being the Point-Spread Function (PSF)

While this model underlines some previous works on Tomo-PIV, in particular the Iterative Particle Reconstruction (IPR) [44], it is only in [4] that it has been used to derive a linear problem suitable for standard inversion algorithms such as MART/SMART.

More precisely, we have demonstrated in [4] that the PVR model of Figure 1 can be approximated by a linear system $I = W\tilde{E}$, where I collects image intensities and the rows of the weighting matrix W are PSF samples $W_{kn} = h(k - n\Delta)$. The 3D field $\tilde{E}$ is a discrete approximate representation of the original Dirac-like particle field, where each particle is represented by a very restricted number of coefficients in neighboring voxels. As such, it is inherently a much sparser representation of the volume than that used in classical Tomo-PIV. Given $\tilde{E}$, the intensity and position of particles can be recovered unambiguously with subvoxel accuracy if they do not overlap. Particle overlapping in 3D space is extremely rare, given the typical values of the number of particles per volume. Thus, it is expected that the reconstructions $\tilde{E}$ will most often truthfully represent the particle distribution. In practice, one usually does not try to recover E and cross-correlate the discrete field $\tilde{E}$ to estimate velocity fields.

We have made comparative studies between two similar SMART algorithms (with MLOS initialization [2]), one, called Tomo-SMART, is based on the conventional Tomo-PIV model of [19] and the other is based on the proposed PVR model and is called PVR-SMART [4]. In all comparisons, PVR-SMART has been shown to increase the performance with respect to Tomo-SMART. For instance, in the simulation study illustrated in Figure 2, PVR-SMART consistently yields

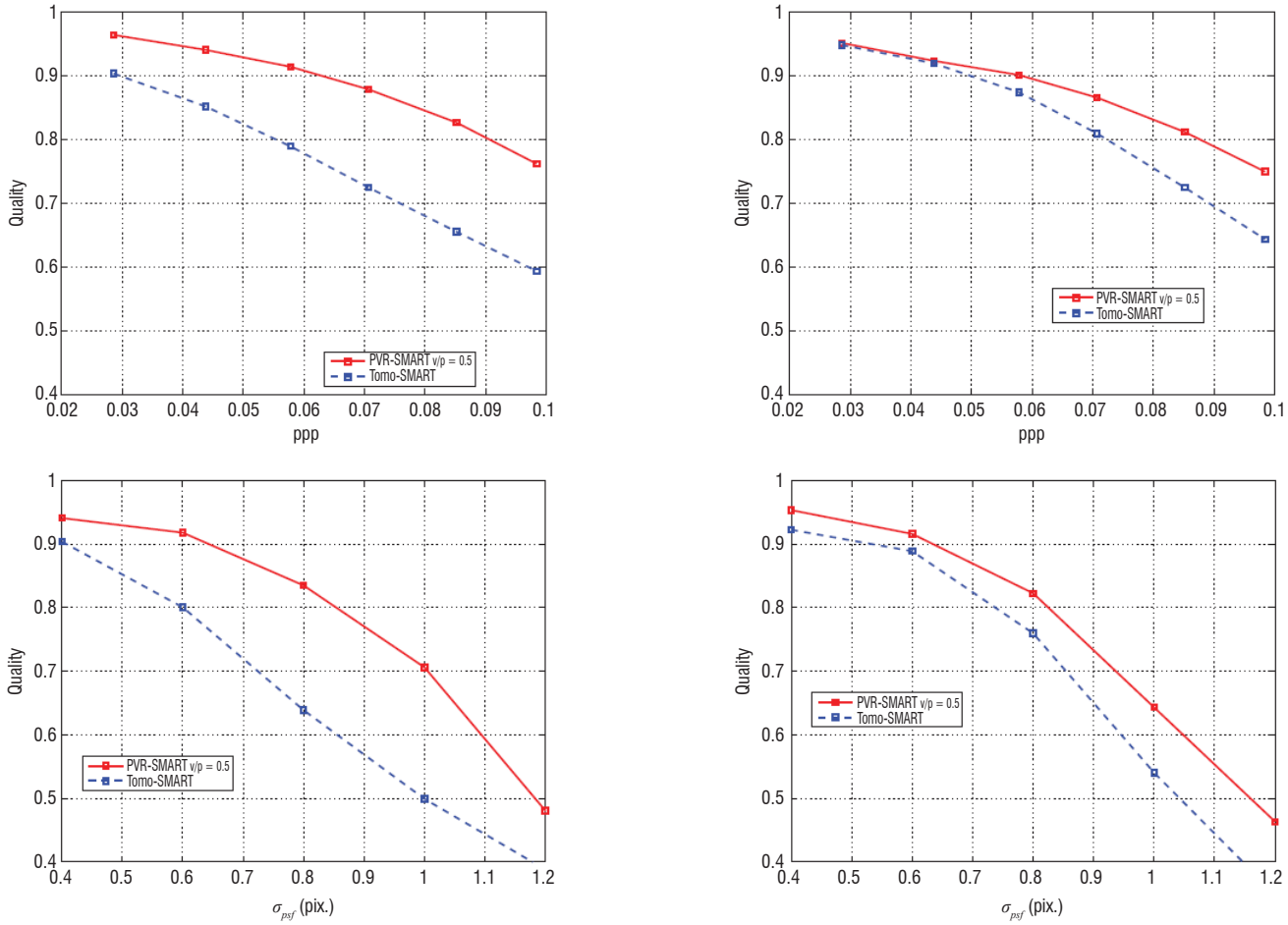

Figure 2 – Comparisons between conventional tomographic reconstruction and the proposed PVR approach, using the SMART algorithm for simulated images (see [4] for details). Top: curves for varying Nppp with $\sigma_{psf} = 0.6$, I/U = 0.47. Bottom: curves for varying σ_{psf} with I/U = 0.47, Nppp = 0.07,. Left: Q criterion of [19]. Right: fraction of detected true particles or Recall

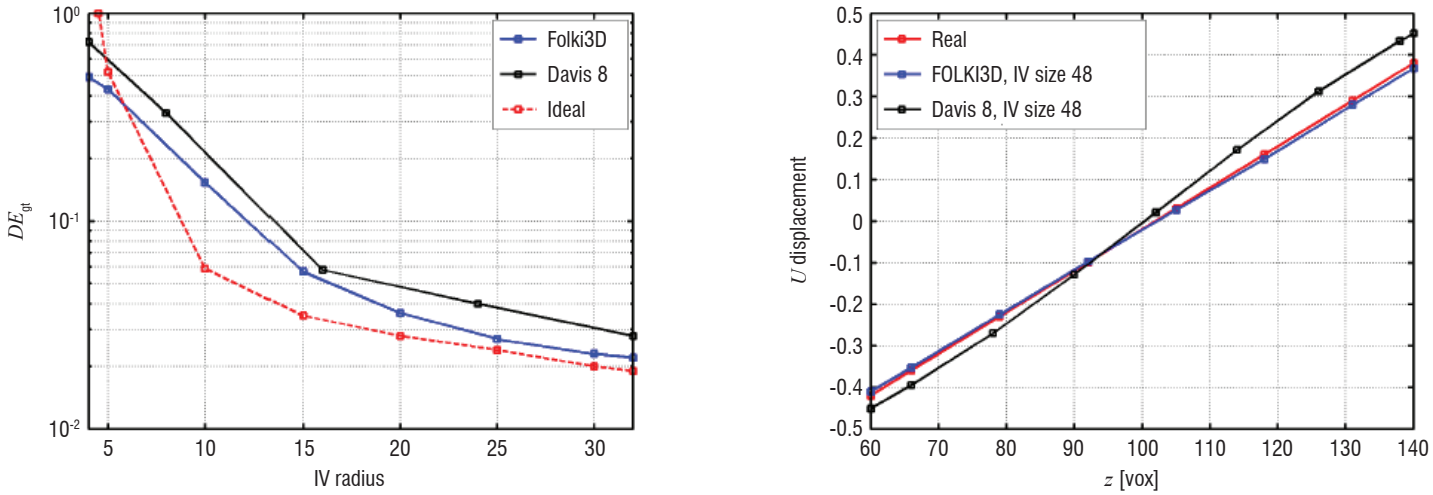

Figure 3 – Comparison of Davis 8.2 and FOLKI3D (IV radius of 24 voxel) on a synthetic shear layer type displacement field $(U,V,W)=(5+\alpha z,0,0)$ with $\alpha = 0.01$. Left: average displacement errors as a function of the IVs radius R – the red curve is FOLKI-3D applied on ground truth volumes. Right: displacement profiles along Z, averaged in the X, Y directions – red represents the true profile

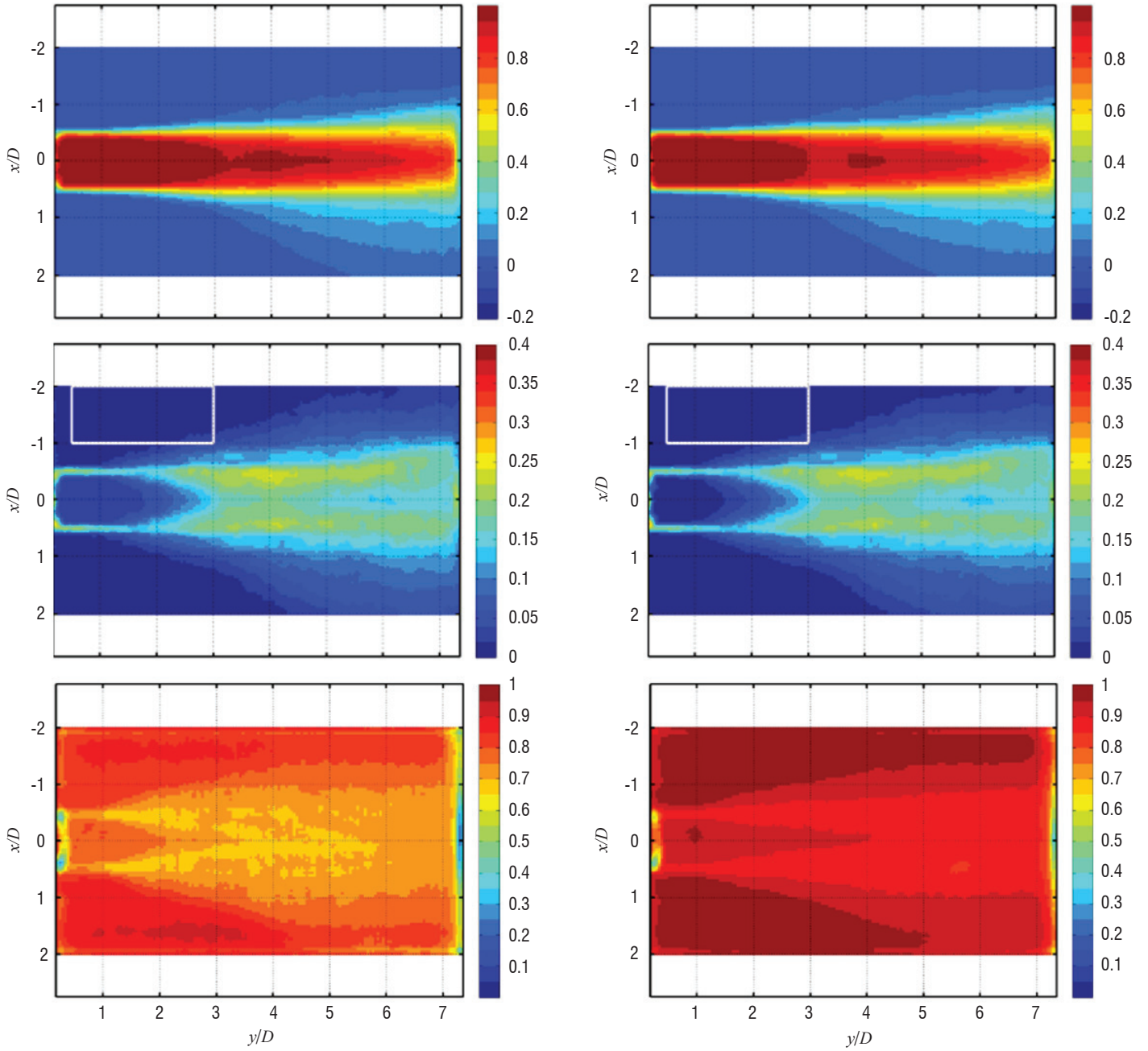

Figure 4 – Comparison of a 3D velocity field estimation by FOLKI3D from Tomo-SMART [19] (Left) and a PVR-SMART tomographic reconstruction (Right) – axial plane $z = 0$. Top to bottom: mean axial velocity, rms of axial velocity, correlation coefficient

better results than Tomo-SMART when varying the ppp (upper row) or the width of the PSF σ_{psf} (lower row). In the sequel, we describe other applications of the PVR model, first to estimate 3D displacement fields from volume correlation, then to derive a sparse approach.

Fast and dense 3D approach: PVR SMART and FOLKI3D

A 3D extension of FOLKI, FOLKI3D, has been proposed and characterized in [6][8]. It shares many characteristics of the 2D method. First, it is a dense calculation that provides the displacement field for all voxels. Second, with respect to the true displacement field, FOLKI3D exhibits a low-pass filter behavior closely related to the shape of the IW. Third, it has a highly parallel structure, allowing very high computational performance on GPUs. This algorithm has been evaluated on simulated volumes, in comparison with the commercial volume correlation software LaVision Davis 8.2. For the selected example, FOLKI3D outperforms Davis 8.2, both in terms of bias (Figure 3, right) and of rms error (Figure 3, left).

Experimental validations have also been conducted on a free round turbulent air jet at a Reynolds number Re = 4500 using a 3D-PIV setup made at ONERA together with a 2D-PIV camera providing reference measurements. The experimental set-up and measurement process, with advanced work concerning synchronization, illumination, seeding, calibration (including PSF calibration) and image preprocessing, are described at length in Ref. [8]. We present here only one comparison of 3D velocity fields, estimated using FOLKI3D from volumes reconstructed either by Tomo-SMART or by PVR-SMART.

Figure 4 first presents the mean velocity estimation (averaged over 300 snapshots). While results appear at first to be quite similar, comparisons of the noise level in regions with a low level of velocity fluctuation (the white rectangle in the images of the middle row) or of the correlation coefficient (last row of Figure 4) reveal that velocity fields estimated from PVR-SMART volumes are significantly less noisy than those estimated from Tomo-SMART. Other evaluations, presented in [8], confirm this difference. It could stem from a higher proportion of ghost particles and/or a higher peak-locking effect in the Tomo-SMART reconstruction method.

We then consider the reconstruction of instantaneous 3D flow structures of the jet, by visualizing selected iso-contours of axial velocity, and of axial and azimuthal vorticity, in Figure 5. Quantities and levels have been chosen so as to highlight the most important features of the jet near-field dynamics, involved in the first stages of mixing. As described for instance in [9][16], fluctuations are mostly dominated by axisymmetric structures of azimuthal vorticity (vortex rings, stemming from the Kelvin-Helmholtz instability), associated with axial velocity fluctuations in the core, and streamwise vortices contained in the mixing layer. When comparing the methods, the global view of the first row indicates that, again, both results are quite consistent. However, looking at the zoomed-in region (lower row of the figure), one can see that PVR-SMART estimates rounder and smoother vortex rings and that the counter-rotating streamwise vortices, which are the key ingredients of jet mixing, appear to be longer, smoother and bigger for PVR-SMART.

To conclude, we have developed an original tomographic PIV pipeline, revisiting the two stages of the classical approach, tomographic reconstruction and 3D correlation. This method is now routinely used at ONERA. Another approach, oriented towards particle localization and tracking, is described below.

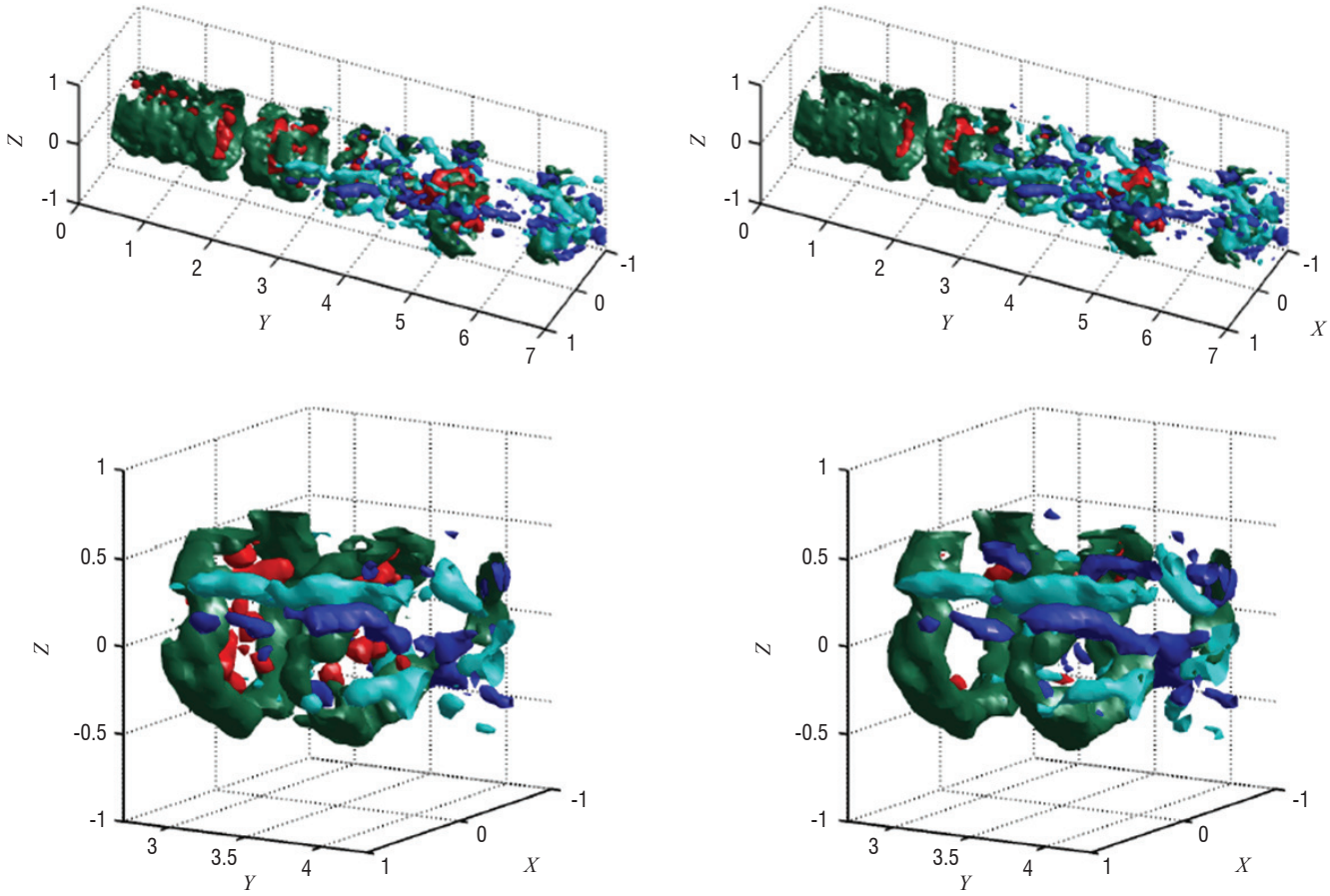

Figure 5 – Reconstruction of instantaneous 3D structures of the jet from Tomo-SMART (left) and PVR-SMART (right) reconstructed volumes. Isovalue of the axial velocity 1.05 V0 (red), Isovalue of the vorticity components $\omega_\theta = 2$ (green), $\omega_z = 1.2$ (cyan) and -1.2 (blue)

Back to particles: an efficient sparse Tomo-PIV on a discretized volume

As a consequence of experimental (seeding density) and numerical choices (spatial discretization), the sought volumes in 3DPIV are very sparse – typical choices lead to a mean density of 1^{-4} particle per voxel. Classical multiplicative algorithms, such as (S)MART, tend to concentrate the energy of the reconstruction on a limited number of "blobs", but they still cannot be considered as exploiting sparsity. Indeed, sparse algorithms are aimed at solving a linear system with a vector (*i.e.*, the discretized volume) having a fixed, limited number of non-zero components (the detected particles). Sparse algorithms have been the subject of important developments within the Signal Processing community, partly motivated by compressed sensing results published in the mid-2000s [18][3]. Few attempts were then made to apply such techniques to tomographic PIV [37][45], but they lead to computationally demanding methods and were applied to small, synthetic volumes. In 2013, based on the PVR model, we proposed the first computationally efficient sparse processing chain for tomographic PIV and demonstrated its performance in terms of the particle detection rate, compared to standard algorithms [10][11].

The initial step is a variation over the classical multiplicative line of sight (MLOS) of [2], where only the local maxima of the MLOS field are retained. Simulation studies have demonstrated that this "LocM" (Local Maximum) strategy allows a drastic reduction of the problem dimensionality, with a limited loss in terms of missed particles. Thus, we propose to solve the Tomo-PIV problem on a discretized 3D grid with a voxel-to-pixel ratio (v/p) equal to 0.5. Using the PVR formulation, the sparse problem concerned is written as

$$\min_E \|WE - I\|^2 \text{ subject to } \|E\|_0 \leq S \qquad (2)$$

where the L0 norm is the number of non-zero components in E, and S, the sparsity number, is the total number of particles in the reconstructed volume. The solution of the previous problem on a discretized 3D grid can be efficiently found with CoSaMP (Compressed Sampling Matching Pursuit) [31]. CoSaMP, a popular algorithm for sparse inversion, builds on the matching pursuit strategy aimed at identifying the support of the solution, *i.e.*, the subset of voxels that contains a particle. This is done by iteratively removing or adding voxels to the current support and using it to solve the problem, *i.e.*, to determine the intensities E_p of the particles that minimize the goodness-of-fit term of (2).

The main parameters of this algorithm, the discretization step and the sparsity number, have been studied in [11]. A discretization step corresponding to a voxel-to-pixel ratio (v/p) equal to 0.5 has been shown to provide a good trade-off between localization accuracy and computation time. The sparsity number can be chosen according to the size of the imaged volume and the seeding density. Comparison with the classical MLOS-SMART approach has also been provided on synthetic and real datasets, showing better performance of LocM-CoSaMP over a large range of seeding densities, as shown in Figure 6.

Two-time-step Tomo-PTV with sparse tomographic reconstruction

From the sparse reconstruction presented before, it is tempting to seek the individual matching of each reconstructed particle from one time instant to the next. This process can be related to PTV (Particle Tracking Velocimetry) [29]. Matching is very ambiguous, because particles are indistinguishable and PTV was traditionally restricted to low seeding density. Recent developments combining an iterative reconstruction algorithm and particle tracking over several time steps [41] have shown interesting results in terms of seeding density. Still, two-time-step PTV remained unsolved for a seeding density higher than 0.005 ppp. In this context, we have proposed a novel "tomoPTV" method, combining all previous results (*i.e.*, PVR model, FOLKI3D and LocM-CoSaMP) [12][13]. We start from the LocM-CoSaMP reconstruction of the particle volume at two time instants. The pointwise LocM-CoSaMP reconstructions are expanded with Gaussian filtering, and a low-resolution first estimation of the 3D displacement field is computed using FOLKI3D. Particle matching is then done by nearest-neighbor search within a limited

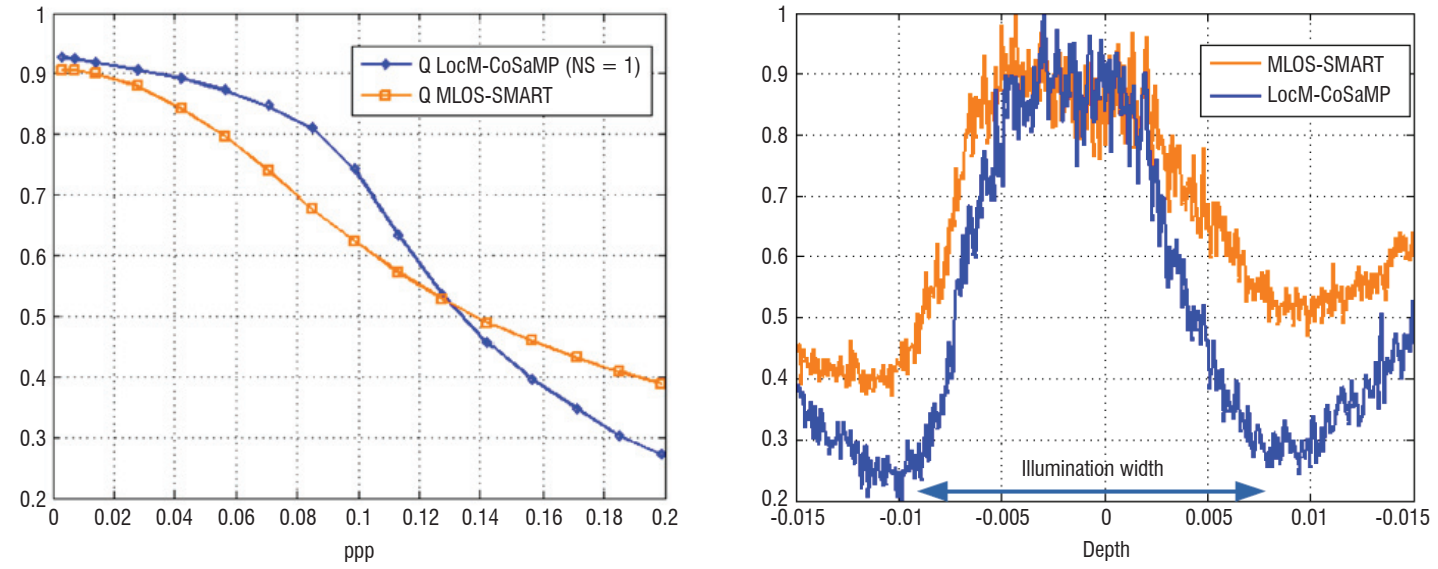

Figure 6 – Comparisons of tomographic reconstructions of volumes of particles using MLOS-SMART (orange colored curves) and LocM-CoSaMP (blue curves). Left: Q-factors [19] in synthetic experiments show that the LocMCoSaMP method outperforms MLOS-SMART on seeding densities up to ppp ≈ 0.12. Right: the Z intensity profiles of reconstructions on real data show a higher R-SNR (ratio between the plateau and edge values) for LocM-CoSaMP, indicating a higher efficiency to preserve real particles and remove ghosts [39]. Details on simulation and experimental conditions are given in [12]

region around the position predicted by FOLKI3D. Finally, subvoxel location of particles is identified by the iterative optimization of

$$\min_{E,X} \sum_j \sum_x \left\{ I_j(x) - \sum_p E_p h\left(x - F_j\left(X_p\right)\right) \right\}^2 \qquad (3)$$

where j refers to the camera index. Changes of location are restricted for each particle to a neighborhood around the discrete position given by the matching process. Note that, contrarily to [44][41], the optimization is done jointly for all particle positions, to account for overlapping particles.

Experimentation on the same low-speed round air jet experiment, as in the previous section, has been carried out to compare classical Tomo-SMART of [19] followed by FOLKI3D to the two-time-step Tomo-PTV technique. Figure 7 presents the U,V components of a slice of the 3D displacement field in the central plane of the jet. It can be seen that the jet structure and the development of its vortical structures (patches of alternate colors that identify Kelvin-Helmholtz azimuthal vortices) in the shear layer are nicely captured by both methods, which yield similar results. This demonstrates the ability of the proposed two-time-step Tomo-PTV technique to yield reliable results with experimental datasets.

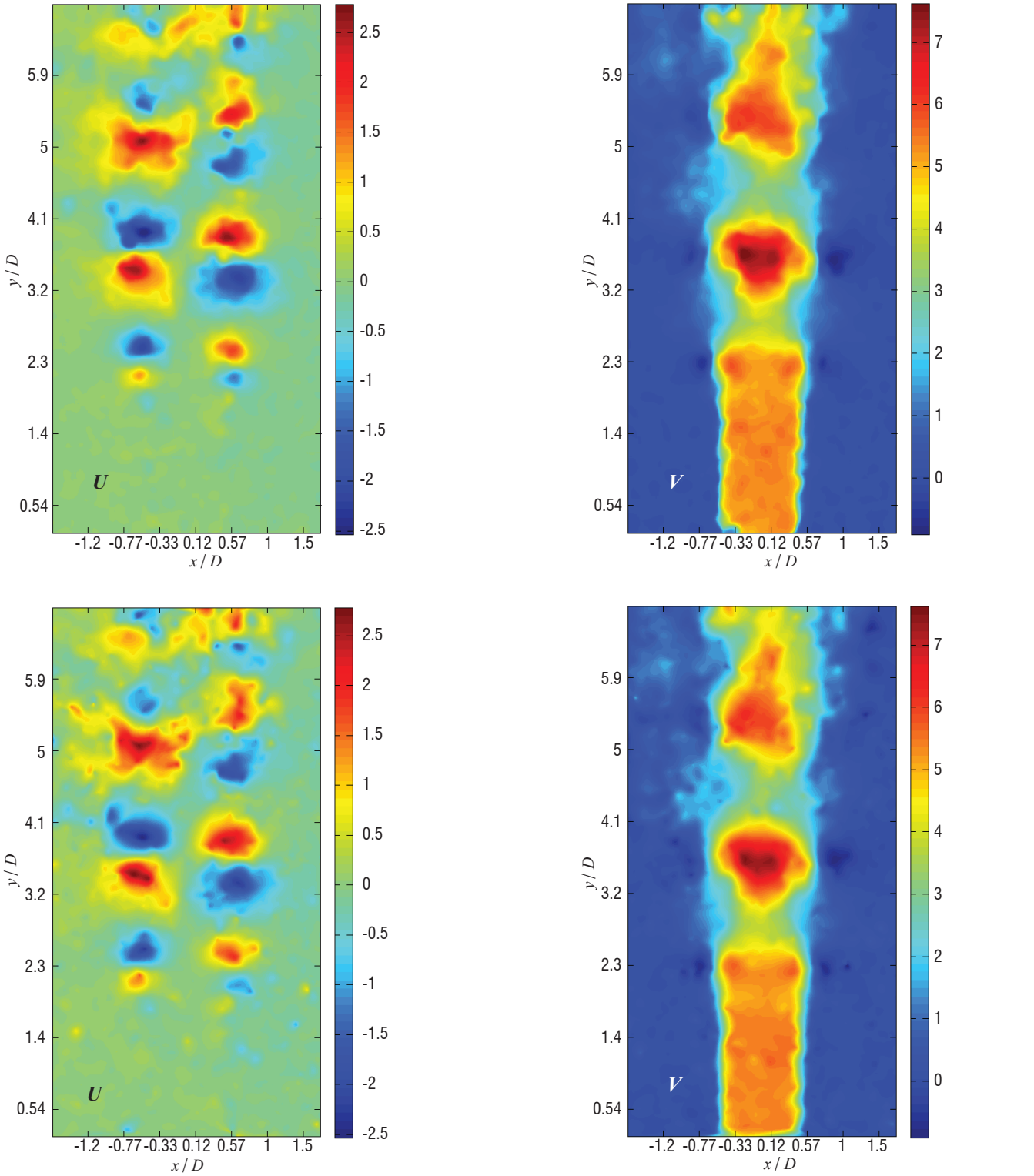

Figure 7 – Displacement fields for a round air jet snapshot. U is collinear to the light propagation and V is collinear to the jet axis. Top: Tomo-SMART of [19] + FOLKI3D; Bottom: LocM-CoSaMP + PTV

A direct method for instantaneous 3DBOS

Introduction

Density field visualization, such as Schlieren techniques, has been used extensively to understand fluid mechanics phenomena such as shock waves or thermal effects. However, the mostly qualitative information resulting from this measurement does not yield enough information to refine computational fluid dynamics codes. Background-oriented Schlieren (BOS) is one way to obtain a quantitative measurement of density gradients [15][30]. It is based on the observation of ray deviations through a medium with inhomogeneous optical index. The BOS optical setting, whose principle is recalled in Figure 8, is remarkably simple: it only requires that the flow under study be placed between a camera and some textured background on which the camera is focused. Comparing the images of the background with and without the flow using digital image correlation techniques reveals displacements, which are the projections of the light ray deviations. Displacement fields are computed by digital image correlation algorithms, here using FOLKI-SPIV [5]. Conversion from displacement to deviation is usually done by approximating the curved ray by two straight lines intersecting at a "deviation point" located somewhere in the reconstructed volume. In the sequel, the deviation point is chosen on the unperturbed ray and equidistant from the entry and exit points.

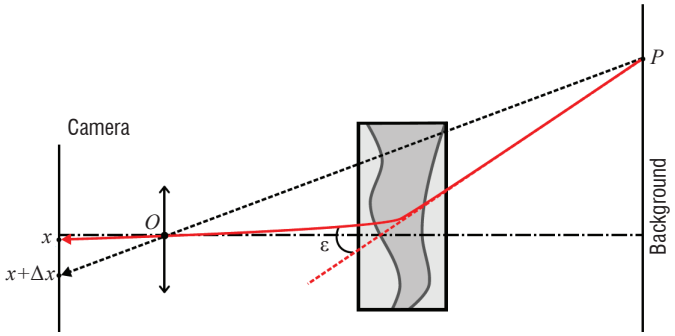

Figure 8 – Principle of BOS measurement: the camera is represented on the left hand side by its center of projection (O), input lens and image plane. It is focused on the background plane on the right. The flow under study, shown in the middle, induces a deviation of the light rays. A point P of the background is imaged at position x with the flow and at $x+\Delta x$ without. Note that the size of the region under study and the ray deviation angle are heavily exaggerated for the sake of clarity

The deviation angle is the main observable of BOS. Considering one ray to be going through the flow under study, the deviation angle ε is equal to the integral of the optical index gradient along the optical path:

$$\varepsilon = \frac{G}{n_0}\int_{ray\subset flow} \nabla\rho(s)\,ds \qquad (4)$$

where n_0 is the optical index outside the flow, and G is the Gladstone-Dale constant which relates the optical index and the density through $n - 1 = G\rho$ (for standard conditions $G = 0.23 * 10^{-3}$ m^3/kg). This problem is generally nonlinear, since the integration path depends on the unknown variable density of the flow. Similar to most other references, we assume a paraxial hypothesis and integration is done along the (straight) unperturbed ray.

A one-step method for 3DBOS reconstruction

If several synchronized cameras are placed all around the flow under study, each one facing a textured background, deviations along several rays passing through the medium with various orientations can be measured. Stacking these deviations in a single observation vector and discretizing Eq. (4), a linear system can be written as:

$$\boldsymbol{\varepsilon} = \begin{bmatrix}\boldsymbol{\varepsilon}_x\\ \boldsymbol{\varepsilon}_y\\ \boldsymbol{\varepsilon}_z\end{bmatrix} = A\rho = T\begin{bmatrix}\boldsymbol{D}_x\\ \boldsymbol{D}_y\\ \boldsymbol{D}_z\end{bmatrix}\rho \qquad (5)$$

3DBOS amounts to inverting this linear system to estimate the discretized density ρ. The observation matrix $\boldsymbol{A}$ is often separated into spatial finite difference approximations of the gradient in each direction (e.g., $\boldsymbol{D}_x$, $\boldsymbol{D}_y$, $\boldsymbol{D}_z$) and a tomographic operator $\boldsymbol{T}$. For this reason, almost all previous references [1][27][36] adopt a two-step inversion scheme, where, first, components of the spatial gradients in all spatial directions are computed by three independent tomographic reconstructions, and, second, density is obtained by spatial integration. The main benefit is to be able to rely on known methods for each step, in particular algorithms originating from Computerized Tomography (CT) for the inversion of $\boldsymbol{T}$. In 2012, we have proposed a direct (or one-step) inversion method that considers the end-to-end observation matrix A [42][32]. In this approach it is easy to use the formalism of regularized inversion by penalization [23], where the density volume is sought as the minimizer of a compound criterion:

$$\mathcal{J} = \|A\rho - \boldsymbol{\varepsilon}\|^2 + \lambda\mathcal{R}(\rho) \qquad (6)$$

Here $\mathcal{R}$ is some regularization term, for instance the L2 norm [32] or L2L1 norm [42] of the spatial gradient of the density volume, and $\lambda > 0$ is a regularization parameter chosen according to an L-curve strategy [22]. Optimization is made with a classical conjugate gradient algorithm, with explicit step computation [42]. It should be mentioned that this problem is of very high dimensions, with typically 107 deviations and 108 reconstructed voxel values, even if we use a user-defined mask to reduce the support of the optimization. The most computationally demanding operations are the application of the observation operator and its adjoint, for instance to compute the gradient of the first term of the criterion $2A^t(A\rho - \boldsymbol{\varepsilon})$. The implementation is derived from the projection and back-projection studied in computerized tomography [21] and makes use of the parallel architecture of the GPU to limit computation time.

This one-step numerical inversion method has been studied on synthetic and real datasets using 12 cameras in Ref. [32]. Non-coplanar configurations of the camera setup were considered, using the Geode experimental bench dedicated to 3DBOS made at ONERA/DMAE (Toulouse) and illustrated in Figure 9 (left image). The experimental results

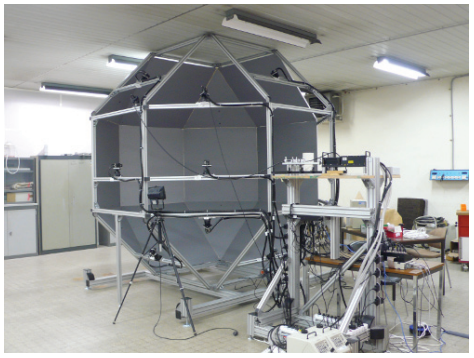

Figure 9 – Left: the "Geode" 3DBOS bench at DMAE allows simultaneous BOS acquisitions from several points of view by up to 12 cameras, each facing a background panel. Right: 3D reconstruction of the plume of a candle with 12 cameras in a 180° planar configuration [32] – Iso-density surfaces at densities 0.7 (red), 0.9 (green) and 1.1 (blue)

have demonstrated the ability of the method to capture complex non-symmetric volumes, such as a candle convective flow or the helicoidal plume of a rotating gas burner, as shown in Figure 9 (right image).

Experimental demonstration of 3DBOS in a research wind tunnel

The 3DBOS technique presented above was demonstrated in a large research wind tunnel in 2014 [34]. The experiment was conducted in ONERA's F2 wind tunnel located in the Fauga-Mauzac center. This subsonic facility can reach a speed of 100 m.s^{-1} and the test section is 1.4 m wide, 1.8 m high and 5 m long. Large window panels provide very good access for optical diagnostics. A combination of screen honeycombs, an acoustics dumper and a contraction ratio of 12 contribute to a turbulence level below 0.05%.

The tested flow is a co-flowing hot jet (with a total temperature of 100°C) generated at the wingtip of a simplified half-wing fixed on the floor of the test section. The upstream wind tunnel flow has a speed of 20 m.s-1 with total temperature and pressure equal to ambient conditions. The 3DBOD system consists of 12 cameras distributed on one side and the ceiling of the test section, the ground and the other side being dedicated to background panels. In parallel, the hot co-flowing jet is also investigated with the stereo PIV technique and thermocouple measurements. In particular, thermal measurements allow a complete comparison with 3DBOS. Figure 10 presents some illustrations of the experimental set-up.

Three-dimensional density fields of the unsteady jet flow have been successfully obtained by the one-step inversion method previously described, as shown in Figure 11 (upper row), and mean density

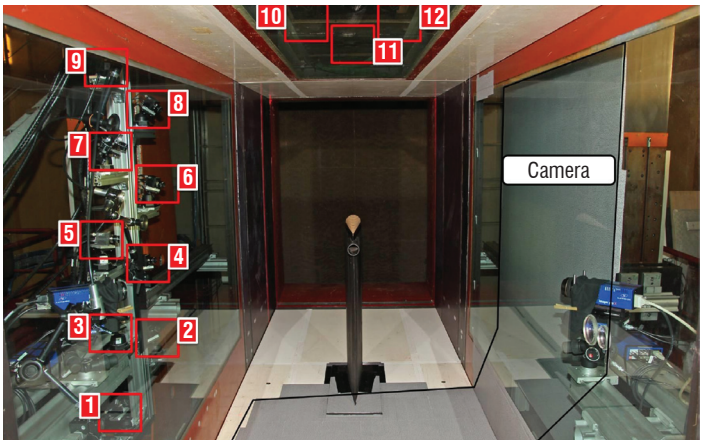

Figure 10 – 3DBOS experiment in ONERA's F2 research wind tunnel (Fauga-Mauzac, France). The twelve cameras are represented with red squares, while the background panels are shown as gray regions. The two cameras of the stereo PIV system are also visible (in blue)

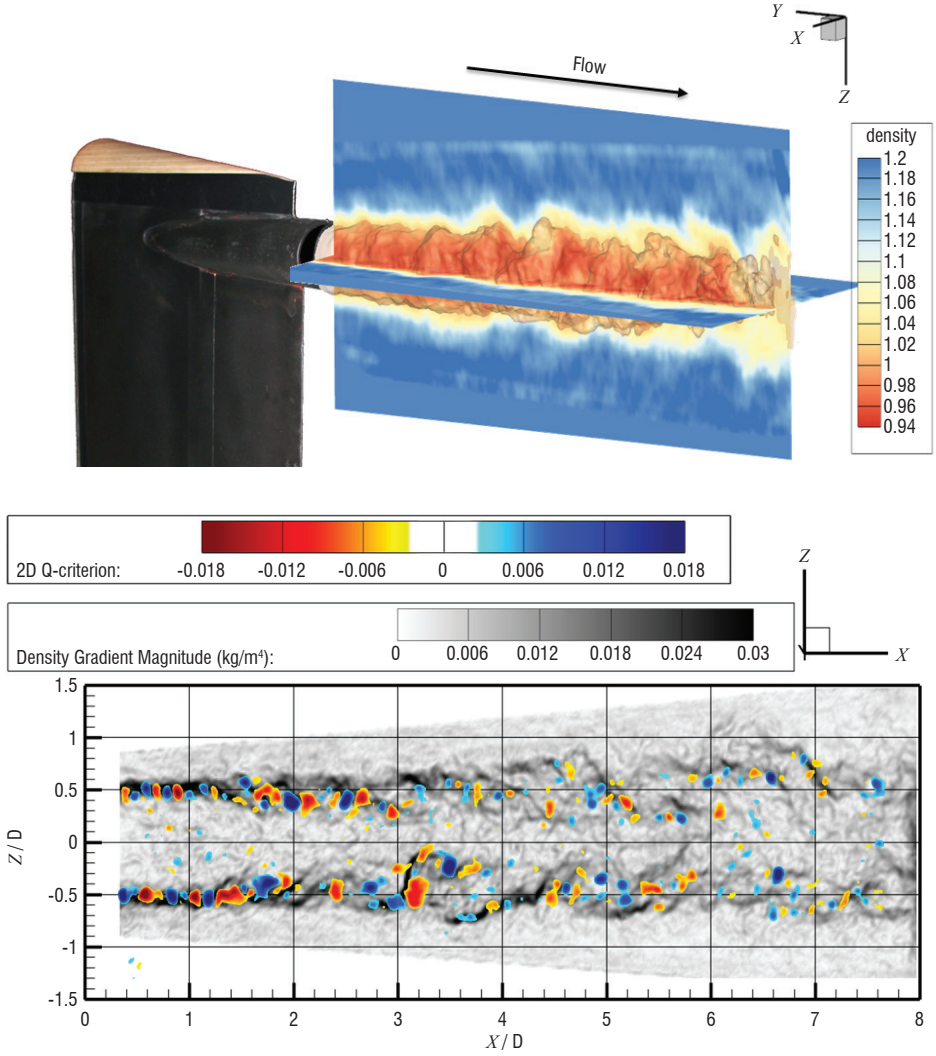

Figure 11 – Instantaneous measurement of a flowing hot jet in ONERA's F2 research wind tunnel. Top: 3DBOS reconstruction of the density field of the unsteady jet flow shown next to the wingtip. Bottom: Density gradient magnitude in gray scale superimposed with the most energetic Q-criterion structures computed on stereo-PIV data. Experimental conditions: Tjet = 100 °C; Qjet = 80 g/s; Vext = 20 m.s^{-1}

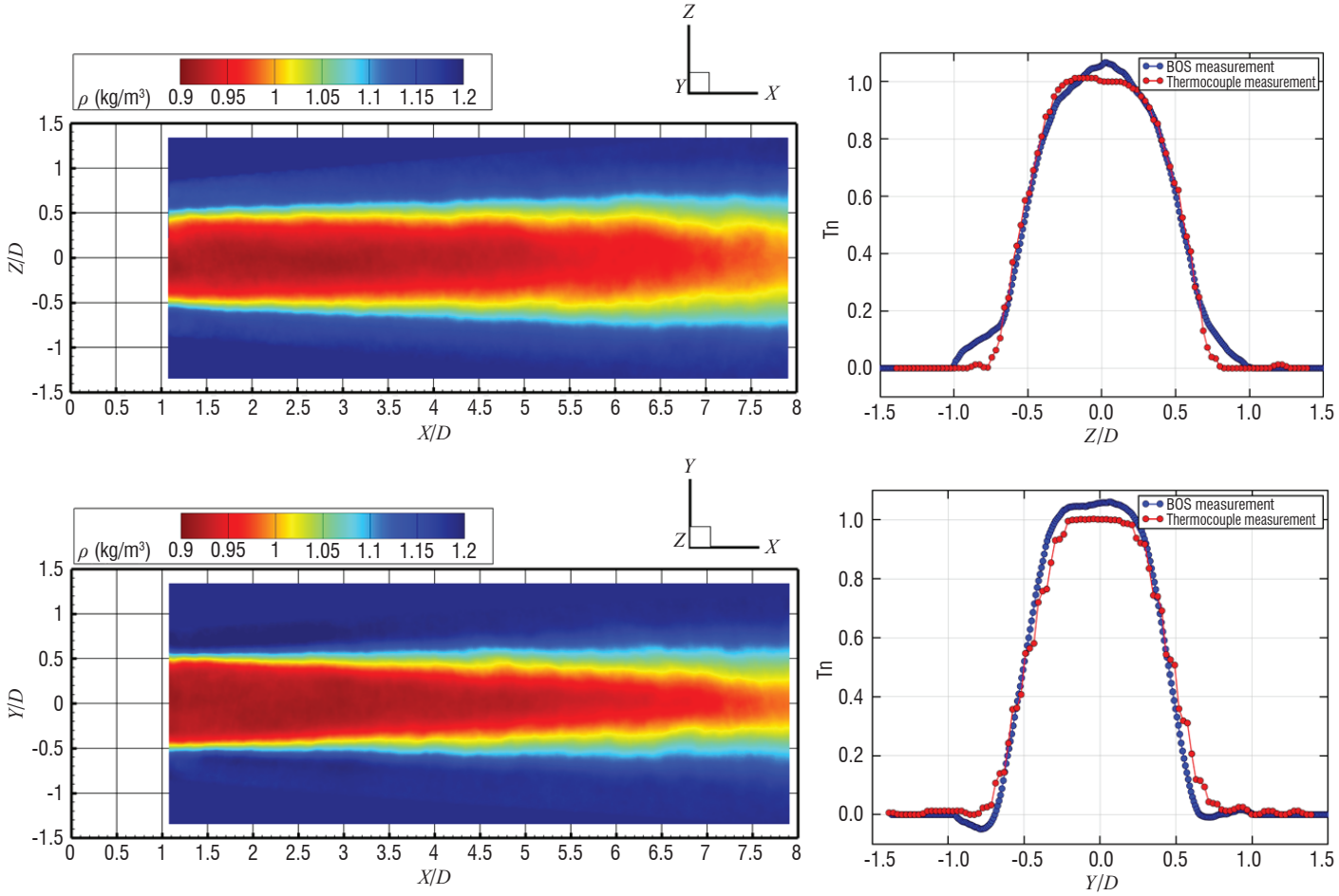

Figure 12 – Mean density reconstructed by 3DBOS and comparison with thermal measurement (Experimental conditions : $V = 20$ m.s^{-1}, $Q = 80$ g.s^{-1}, Tjet $= 100$°C). Left column: Longitudinal profiles of the averaged density field (top: $Y = 0$; bottom: $Z = 0$). Right column: normalized temperature profiles from 3DBOS and from thermocouples (top: vertical; bottom: horizontal) in the $X/D = 2.8$ slice.

fields reconstructed on a 116 Megavoxel volume with a spatial resolution of 0.5 mm are presented in Figure 12 (left column).

In this configuration, the influence of pressure on density can be neglected and temperature maps can then be extracted directly from the density field. Both measurements are compared on a mean flow field in Figure 2, using a normalized temperature to account for the changes in the wind tunnel flow external temperature (see details in Ref. [34]). This comparison shows a very good agreement between both techniques. The small overprediction in temperature noticed for the BOS measurement is below the thermocouple measurement uncertainty. This shows the potential of 3DBOS for providing the full 3D temperature field in non-compressible flows with known pressure distribution.

Moreover, Figure 11 (bottom row) presents a superimposition of the instantaneous stereo-PIV and 3DBOS results illustrated, respectively, by the Q-criterion and the density gradient magnitude maps in the same plane. Note that the 3DBOS results have been obtained with only 9 cameras, in order to avoid reciprocal illumination effects of the two measuring systems. However, the degradation in spatial resolution is limited within the visualization plane. This representation nicely emphasizes that the most energetic Q-criteria are located in the mixing layer around the Kelvin-Helmholtz windings revealed by BOS.

Achieving 3DBOS reconstruction of compressible flows

Our main concern is now the extension of the proposed 3DBOS method to flows with higher density gradients, which are responsible for strong and highly inhomogeneous blurring effects in recorded images. Nevertheless, we have been able, thanks to a refined model of the observation and careful choice of experimental conditions, to produce deviation maps with a spatial resolution comparable to that of Schlieren visualization, as illustrated in Figure 13.

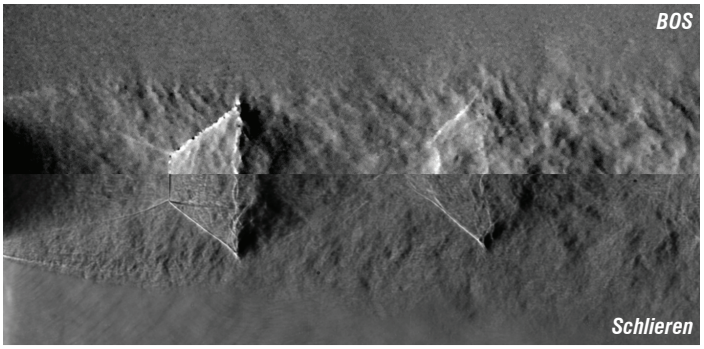

Figure 13 – Experimental images of an under-expanded jet with NPR = 5. With a careful choice of the experimental conditions, the BOS deviation image (top half-image) exhibits a spatial resolution comparable to that of traditional Schlieren (bottom half-image)

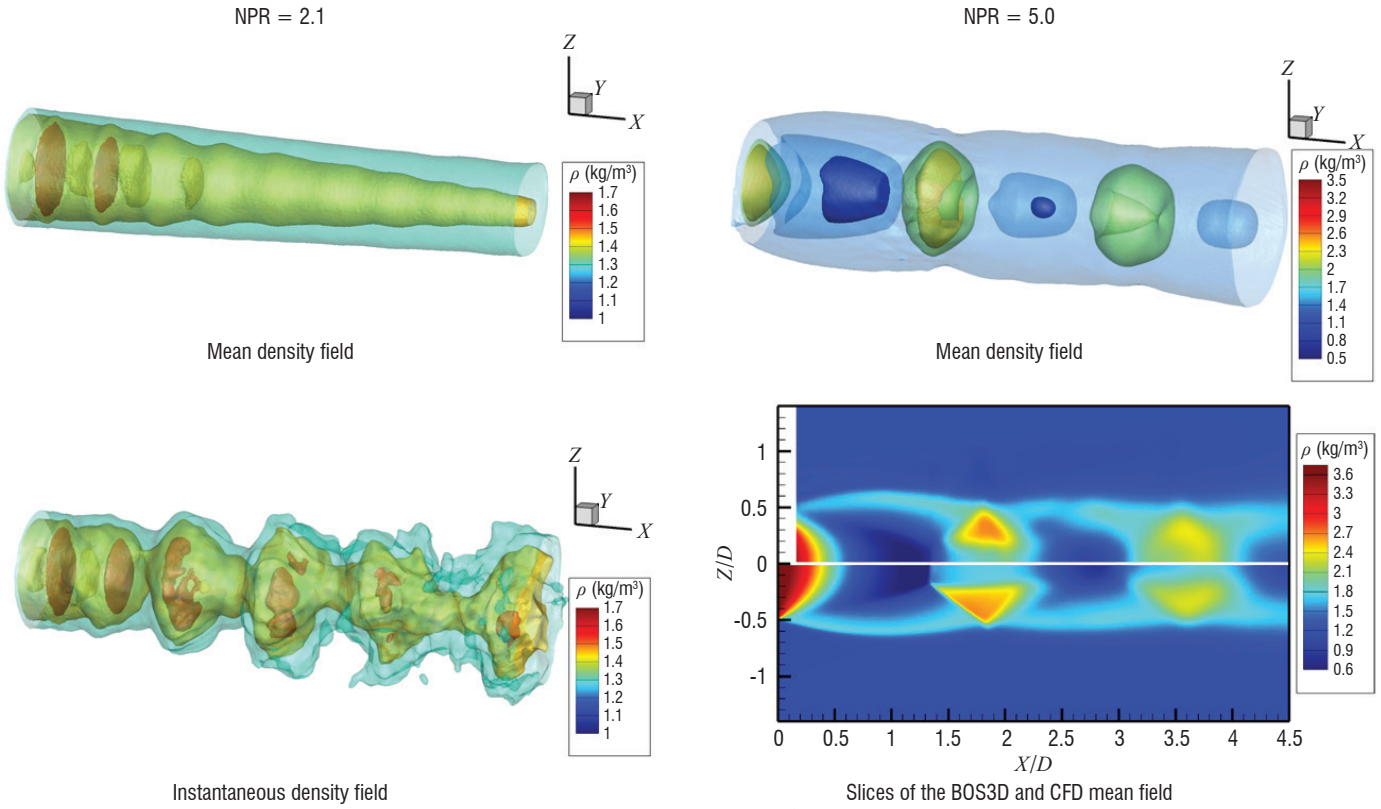

Figure 14 – 3DBOS reconstruction of the density field of an under-expanded flow with NPR = 2.1 (left column) and NPR = 5 (right column). Top row: mean density field from 900 recordings. Bottom right: instantaneous density field for NPR = 2.1. Bottom left: comparison of 3DBOS and CFD mean density field for NPR = 5.0. The calculations are done over volumes of 10 x 7 x 7 cm³ using between 40 and 100 million 0.2 mm-side voxels. More details can be found in [33].

However, contrarily to Schlieren techniques, BOS measurement opens the way to quantitative 3D reconstruction of the flow. In a very recent demonstration [33], the 3DBOS reconstruction technique presented above was applied to deviation data produced by a dedicated 12-camera bench on a underexpanded jet with variable nozzle pressure ratio (NPR). Figure 14 shows results for NPR = 2.1 and NPR=5.0, with 3D mean density field on the top row. In the NPR = 2.1 case, the train of shock waves is clearly visible in the potential core region. The two first shocks are found in the instantaneous flow (bottom left image), while the jet topology is much more complex further downstream as it becomes destabilized. For NPR = 5, a Mach disk is clearly visible. The 3DBOS reconstruction shows a very good agreement with a DNS simulation. Both the density levels and the flow topology are well recovered, with a consistent location of the Mach disk and shock-cells. To the best of our knowledge, these reconstructions of under-expanded flows presented here and in Ref. [33] have never been obtained before.

Perspectives

Thanks to a joint investment by three scientific departments, 3DPIV and 3DBOS are now mastered at ONERA. To the best of our knowledge, our 3DBOS reconstructions of instantaneous flows have no equivalent in the published literature of experimental fluid mechanics. With regard to 3DPIV, our developments have many more competitors, however, the very recently released results of the 4th PIV Challenge [24] indicate that our results are among the best (for Case C of the Challenge).

This paper focuses on the underlying numerical developments; let us emphasize that several other skills have been acquired along the way, particularly in terms of experimental methodology, relating to subjects such as camera set-up, seeding techniques and background design, illumination tools, camera models, calibration methods, estimation error sources, etc. Some of these advances have already been published [7][8][14][34][26][32] and others will be the subject of future publications.

The perspectives of 3DPIV include algorithmic development for temporal processing, either according to the dense correlation paradigm, as a 3D extension of our recent proposal [46], or within the particle tracking framework in line with [41]. As regards 3DBOS, we are working on a new direct model and associated estimation methods for high gradients or shock wave situations. In this context, we are also currently comparing 3DBOS with other optical measurement methods, such as digital holography [17][35].

As illustrated in Figure 11, joint 3D BOS and PIV measurements have already been conducted: further investigations in this line are planned for the experimental study of compressible flows, a domain where imaging measurement techniques are challenged by aero-optical effects. The information contributed by BOS could be useful for more accurate velocimetry, for instance.

Finally, 3D field measurement is also a gateway towards tighter coupling between experiments and numerical simulations, a field which we believe will be of major importance in future aerodynamic studies ■

References

[1] B. ATCHESON, I. IHRKE, W. HEIDRICH, *et al.* - *Time-Resolved 3D Capture of Non-Stationary Gas Flows*. ACM Transactions on Graphics (TOG), ACM, 2008. p. 132.

[2] C. ATKINSON, J. SORIA - *An Efficient Simultaneous Reconstruction Technique for Tomographic Particle Image Velocimetry.* Experiments in Fluids, 2009, vol. 47, no 4-5, p. 553-568.

[3] E. J. CANDÈS - *Compressive sampling*. Proceedings of the International Congress of Mathematicians, 2006, p. 1433-1452.

[4] F. CHAMPAGNAT, P. CORNIC, A. CHEMINET, *et al.* - *Tomographic PIV: Particles Versus Blobs*. Measurement Science and Technology, 2014, vol. 25, no 8, p. 084002.

[5] F. CHAMPAGNAT, A. PLYER, G. LE BESNERAIS, *et al*. - *Fast and Accurate PIV Computation Using Highly Parallel Iterative Correlation Maximization*. Experiments in Fluids, 2011, vol. 50, no 4, p. 1169-1182.

[6] A. CHEMINET, B. LECLAIRE, F. CHAMPAGNAT, *et al*. - *Accuracy Assessment of a Lucas-Kanade Based Correlation Method for 3D PIV.* 17th International Symposium on Applications of Laser Techniques to Fluid Mechanics, 2014.

[7] A. CHEMINET, B. LECLAIRE, F. CHAMPAGNAT, *et al*. - *On Factors Affecting the Quality of Tomographic Reconstruction*. PIV13, 10th International Symposium on Particle Image Velocimetry, Delft, The Netherlands, July 1-3, 2013.

[8] A. CHEMINET - *Tomographic PIV Development for the Study of Turbulent Flows*. PhD dissertation, Université Paris-Saclay, 2016.

[9] J. H. CITRINITI, W. K. GEORGE - *Reconstruction of the Global Velocity Field in the Axisymmetric Mixing Layer Utilizing the Proper Orthogonal Decomposition*. Journal of Fluid Mechanics, 2000, vol. 418, p. 137-166.

[10] P. CORNIC, F. CHAMPAGNAT, A. CHEMINET, *et al*. - *Computationally Efficient Sparse Algorithms for Tomographic PIV Reconstruction.* PIV13, 10th International Symposium on Particle Image Velocimetry, Delft, The Netherlands, July 1-3, 2013.

[11] P. CORNIC, F. CHAMPAGNAT, A. CHEMINET, *et al.* - *Fast and Efficient Particle Reconstruction on a 3D Grid Using Sparsity*. Experiments in Fluids, 2015, vol. 56, no 3, p. 1-7.

[12] P. CORNIC, F. CHAMPAGNAT, A. PLYER, B. LECLAIRE, A. CHEMINET and G. LE BESNERAIS - *Tomo-PTV with Sparse Tomographic Reconstruction and Optical Flow*. 17th International Symposium on Applications of Laser Techniques to Fluid Mechanics, Lisbon, 2014.

[13] P. CORNIC, B. LECLAIRE, A. CHEMINET, *et al*. - *Two Time Steps Tomo-PTV with Sparse Tomographic Reconstruction Versus Tomo-PIV*. PIV15, 11th International Symposium on Particle Image Velocimetry, Santa Barbara (California, USA), 2015.

[14] P. CORNIC, C. ILLOUL, Y. LE SANT, *et al*. - *Calibration Drift within a Tomo-PIV Setup and Self-Calibration*. PIV15, 11th International Symposium on Particle Image Velocimetry, Santa Barbara (California, USA), 2015.

[15] S. B. DALZIEL, G. O. HUGHES and B. R. SUTHERLAND - *Whole-Field Density Measurements by "Synthetic Schlieren".* Experiments in Fluids, 2000, vol. 28, no 4, p. 322-335.

[16] S. DAVOUST, L. JACQUIN, B. LECLAIRE - *Dynamics of m=0 and m=1 Modes and of Streamwise Vortices in a Turbulent Axisymmetric Mixing Layer*. Journal of Fluid Mechanics, 2012, vol. 709, p. 408-444.

[17] J.-M. DESSE, P. PICART and P. TANKAM - *Digital Three-Color Holographic Interferometry for Flow Analysis.* Optics Express, 2008, vol. 16, no 8, p. 5471-5480.

[18] D. L. DONOHO - *Compressed Sensing*. IEEE Transactions on Information Theory, 2006, vol. 52, no 4, p. 1289-1306.

[19] G. E. ELSINGA, F. SCARANO, B. WIENEKE, *et al*. - *Tomographic Particle Image Velocimetry.* Experiments in Fluids, 2006, vol. 41, no 6, p. 933-947.

[20] G. E. ELSINGA, J. WESTERWEEL, F. SCARANO, *et al*. - *On the Velocity of Ghost Particles and the Bias Errors in Tomographic-PIV.* Experiments in fluids, 2011, vol. 50, no 4, p. 825-838.

[21] N. GAC, A. VABRE, A. MOHAMMAD-DJAFARI, *et al*. - *GPU Implementation of a 3D Bayesian CT Algorithm and its Application on Real Foam Reconstruction*. The First International Conference on Image Formation in X-Ray Computed Tomography, 2010, p. 151-155.

[22] P. C. HANSEN - *Analysis of Discrete Ill-Posed Problems by Means of the L-Curve*. SIAM review, 1992, vol. 34, no 4, p. 561-580.

[23] J. IDIER - *Bayesian approach to Inverse problems*. 2010, vol. 35, Wiley, New York.

[24] C. KAHLER, T. STARITA, P. P. VLACHOS, *et al.* - *Main Results of the 4th International PIV Challenge*. Experiment in Fluids, may 2016.

[25] G. LE BESNERAIS, F. CHAMPAGNAT, A. PLYER, *et al*. - *Advanced Processing Methods for Image-Based Displacement Field Measurement.* AerospaceLab, 2009, no 1, p. 1-12.

[26] Y. LE SANT, V. TODOROFF, A. BERNARD-BRUNEL, *et al*. - *Multi-Camera Calibration for 3DBOS*. 17th International Symposium on Applications of Laser Techniques to Fluid Mechanics, 2014.

[27] B. LECLAIRE, C. BROSSARD, R. COURTIER, *et al*. - *Particle Image Velocimetry : a Key Contributor to Aerospace Research*. Aerospace Lab, 2016.

[28] F. LEOPOLD, M. OTA, D. KLATT, *et al*. - *Reconstruction of the Unsteady Supersonic Flow Around a Spike Using the Colored Background Oriented Schlieren Technique*. J. Flow Control Measur. Vis., 2013, 1(2):69-76.

[29] H. G. MAAS, A. GRUEN and D. PAPANTONIOU - *Particle Tracking Velocimetry in Three-Dimensional Flows*. Experiments in Fluids, 1993, vol. 15, no 2, p. 133-146.

[30] G. MEIER - *Computerized Background-Oriented Schlieren*. Experiments in Fluids, 2002, vol. 33, no 1, p. 181-187.

[31] D. NEEDELL and J. A. TROPP - *CoSaMP: Iterative Signal Recovery from Incomplete and Inaccurate Samples*. Applied and Computational Harmonic Analysis, 2009, vol. 26, no 3, p. 301-321.

[32] F. NICOLAS, V. TODOROFF, A. PLYER, *et al*. - *A Direct Approach for Instantaneous 3D Density Field Reconstruction from Background-Oriented Schlieren (BOS) Measurements*. Experiments in Fluids, 2016, vol. 57, no 1, p. 1-21.

[33] F. NICOLAS, D. DONJAT, O. LEON, *et al*. - *3D Reconstruction of Compressible Flow by Synchronized Multi-Camera BOS*. Submitted to Experiments in Fluids (2nd revision), dec. 2016.

[34] F. NICOLAS, D. DONJAT, A. PLYER, *et al*. - *Experimental Study of a Co-Flowing Jet in ONERA's F2 Research Wind Tunnel by 3D Background Oriented Schlieren*. Submitted in Meas. Sci. Technol., dec. 2016.

[35] F. OLCHEWSKY, J.-M. DESSE, F. NICOLAS, *et al.* - *3D Reconstruction of Helium Jet by Multidirectional Polarized White Light Differential Interferometry*. Symposium on Flow Visualization, Knoxville, USA, 2016.

[36] K. OTA and M. HAMADA - *Quantitative 3D Density Measurement of Supersonic Flow by Colored Grid Background Oriented Schlieren Technique.* ICAS, 2010, p. 23.

[37] S. PETRA and C. SCHNÖRR - *Tomo-PIV Meets Compressed Sensing*. Pure Math Appl., 20(1-2):49-76 2009.

[38] M. RAFFEL, C. WILLERT, S. WERELEY, *et al*. - *Particle Image Velocimetry: a Practical Guide*. Springer, 2007.

[39] F. SCARANO - *Tomographic PIV: Principles and Practice*. Measurement Science and Technology, 2013, vol. 24.

[40] D. SCHANZ, S. GESEMANN, A. SCHRÖDER, *et al*. - *Non-Uniform Optical Transfer Functions in Particle Imaging: Calibration and Application to Tomographic Reconstruction*. Measurement Science and Technology, 2012, vol. 24, no 2.

[41] D. SCHANZ, A. SCHRÖDER, S. GESEMANN, *et al*. - *"Shake The Box": A highly Efficient and Accurate Tomographic Particle Tracking Velocimetry (TOMO-PTV) Method Using Prediction of Particle Positions.* PIV13, 10th International Symposium on Particle Image Velocimetry, Delft, The Netherlands, July 1-3, 2013.

[42] V. TODOROFF, G. LE BESNERAIS, D. DONJAT, *et al*. - *Reconstruction of Instantaneous 3D Flow Density Fields by a New Direct Regularized 3DBOS Method*. 17th International Symposium on Applications of Laser Techniques to Fluid Mechanics, Lisbon, 2014.

[43] D. VIOLATO and F. SCARANO - *Three-Dimensional Evolution of Flow Structures in Transitional Circular and Chevron Jets*. Physics of Fluids (1994-present), 2011, vol. 23, no 12, p. 124.

[44] B. WIENEKE - *Iterative Reconstruction of Volumetric Particle Distribution.* Measurement Science and Technology, 2012, vol. 24, no 2, p. 024008

[45] Z. YE, Q. GAO, H. WANG, *et al.* - *Dual-Basis Reconstruction Techniques for Tomographic PIV*. Science China Technological Sciences, 2015, vol. 58, no 11, p. 1963-1970.

[46] R. YEGAVAN, B. LECLAIRE, F. CHAMPAGNAT, *et al*. - *Lucas-Kanade Fluid Trajectories for Time-Resolved PIV*. Accepted in Measurement Science and Technology, 2016.

AUTHORS

Guy Le Besnerais graduated from ENSTA in 1989 and obtained his PhD degree from *Université Paris Sud* in 1993. Since 1994, he has been working in the Information Processing and Modeling Department at ONERA, the French Aerospace Lab. He obtained the degree of *Habilitation à Diriger les Recherches* (HDR) in 2008 and is affiliated to Paris-Saclay University. Since October 2016, he is a Research Director at ONERA. His research activities include methods for solving inverse problems, performance modeling for imaging measurement systems, and embedded vision for robotics applications.

Frédéric Champagnat graduated from ENSTA in 1989 and obtained his PhD degree from *Université Paris Sud* in 1993. Since 1999 he has been working in the Information Processing and Modeling Department at ONERA, the French Aerospace Lab. Since 2010, he has been a senior scientist and achieved the degree of *Habilitation à Diriger les Recherches* (HDR) in 2011. He is affiliated to Paris-Saclay University and is a member of the board of the first Comité de Pôle of the STIC doctorate school. His research activities include stochastic modeling of signals and images, methods for solving inverse problems, image deblurring and super-resolution and performance modeling for imaging measurement systems. His work is applied in video processing, satellite and airborne imaging, metrology by imaging in fluid mechanics, and the co-design of hybrid sensor+processing systems.

Philippe Cornic graduated from the *École Nationale Supérieure des Ingénieurs Electriciens de Grenoble* in 1989. He has been working on computer vision at ONERA since 1992 and is currently a senior research engineer. His main research interests are geometric computer vision (image to model registration, video and image georeferencing, etc.) and tomographic methods for estimating scalar (BOS) or vector (Particle Image Velocimetry) fields for Fluid Mechanics.

Aurélien Plyer graduated from *Université Pierre et Marie Curie* (Paris 6) in 2008 and received his PhD degree in Image Processing from the *Université de Paris XIII*, in 2013. He is now working in the Information Processing and Modeling Department at ONERA, the French Aerospace Lab. His research deals with high efficiency parallel methods for low-level video processing and 3D environment perception, with application to robotics and experimental physics.

Benjamin Leclaire graduated from the *École Polytechnique*, France, in 2001. He obtained his PhD degree in Fluid Mechanics in 2006. He is now both a researcher at ONERA and an assistant professor at the *École Polytechnique*. His research interests include optical metrology for fluid dynamics, and turbulent flows.

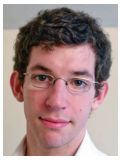

Adam Cheminet graduated from *ENS Cachan*, France, in 2011. He defended his PhD in Fluid Mechanics in May 2016. He is now an ATER at *Université Pierre et Marie Curie*, Paris VI, teaching at undergraduate levels and carrying out research at Institut Jean le Rond d'Alembert-UPMC. His research interests focus on turbulent flows, ranging from optical metrology for fluid dynamics to numerical models for numerical simulation of turbulent flows.

Cédric Illoul joined ONERA in 2012 as a technician for the use and development of optical methods such as PIV, PSP (Pressure Sensitive Paint). He is in charge of assessing new devices, such as using high-power LED for optical methods.

Gilles Losfeld joined ONERA in 1965 as a technician in a supersonic wind tunnel. He then became a member of the ONERA team that developed LDV (Laser Doppel Velocimetry) at ONERA in the early 70's. He has gained a lot of experience and skill in optical methods, such as Schlieren and methods that use laser systems. He is the head of the group within the DAFE department that develops and uses these methods for wind tunnel testing.

Yves Le Sant has been a researcher at ONERA since 1983. His first studies concerned wall interferences and the development of an adaptive test section. He then became involved in applying and developing numerous measurement methods, such as heat flux assessment, Temperature and Pressure Sensitive Paints and the Model Deformation Method. His current activities are in the field of image processing applications, such as Particle Image Velocimetry, and using modern parallel computing architectures such as GPU.

François Nicolas graduated from the *École Nationale Supérieure de Mécanique et d'Aérotechniques* (ENSMA) in Poitiers and received a Master's Degree in mechanical and aerospace engineering in 2013. He achieved his PhD at ONERA Toulouse contributing to the development of 3DBOS and the use of the technique in wind tunnels. He is now in charge of aeroacoustics development for the ONERA large wind tunnel facilities.

Dr. David Donjat graduated from IUSTI in Marseille and received his PhD degree in 2003. From 2003 to 2006 he worked mainly on aerothermal activities, including antiicing systems and internal aerothermal management for Aeroconseil and Airbus. In 2006, he joined ONERA's DMAE department where he currently works on new experimental methods, such as 3DBOS for aerothermal flow characterization and modeling.

After a doctoral degree in Poitiers University, **Francis Micheli** worked with the DAFE's (Fundamental and Experimental Aerodynamics Department) Laser Velocimetry team from 1990 to 2003. He was project leader for LDV measurement campaigns in the Meudon center, with experimental conditions ranging from low velocity to high supersonic. Since 2003, he works in the DMAE (Aerodynamics and Energetics Modeling Department), both with the aeroacoustic and aero-thermal teams. His work mainly concerns the LDV measurements, with contributions in BOS experiments within small or large wind tunnels and more recently about instrumentation on flame test bench.